Title
Conductivity of Block Copolymer Electrolytes Containing Lithium Polysulfides

Journal
Macromolecules, 48(14)

ISSN
0024-9297

Authors
Wang, Dunyang Rita
Wujcik, Kevin H
Teran, Alexander A
et al.

Publication Date
2015-07-28

DOI
10.1021/acs.macromol.5b00928

Peer reviewed

Macromolecules

Article

pubs.acs.org/Macromolecules

Conductivity of Block Copolymer Electrolytes Containing Lithium Polysulfides

Dunyang Rita Wang,[†,∥] Kevin H. Wujcik,[‡,§] Alexander A. Teran,[‡,§] and Nitash P. Balsara*[,‡,§,∥]

[†]Department of Materials Science and Engineering and [‡]Department of Chemical and Biomolecular Engineering, University of California, Berkeley, Berkeley, California 94720, United States

[§]Environmental Energy Technologies Division and [∥]Materials Sciences Division, Lawrence Berkeley National Laboratory, Berkeley, California 94720, United States

Supporting Information

ABSTRACT: Lithium−sulfur batteries are attractive due to their high theoretical specific energy, but the dissolution of lithium polysulfide intermediate species formed during discharge results in capacity fade and limited cycle life. In this study we present the first measurements of ionic conductivity of the polysulfides in a nanostructured block copolymer. The morphology, thermal properties, and the conductivities of polystyrene-*b*-poly(ethylene oxide) (SEO) containing lithium polysulfides, Li_2S_x (x = 4, 8), were studied using small-angle X-ray scattering (SAXS), differential scanning calorimetry (DSC), and ac impedance spectroscopy. We also measured conductivities of mixtures of poly(ethylene oxide) (PEO) and Li_2S_x. X-ray absorption spectroscopy was used to confirm the nature of dissolved polysulfides. SAXS measurements on SEO/Li_2S_x mixtures indicated that all samples had a lamellar morphology. DSC measurements indicated that SEO/Li_2S_8 interactions were more favorable than SEO/Li_2S_4 interactions. The effect of nanostructure on transport of Li_2S_x was quantified by calculating a normalized conductivity, which is proportional to the ratio of the conductivity of SEO/Li_2S_x to that of the PEO/Li_2S_x. The normalized conductivities of both polysulfides peaked at intermediate concentrations. The efficacy of block copolymer electrolytes in Li−S batteries was evaluated by comparing ionic conductivities of polymer electrolytes containing Li_2S_x with those containing lithium bis(trifluoromethanesulfonyl)imide (LiTFSI), a common salt used in PEO-based battery electrolytes. The transport of Li_2S_x species in SEO is suppressed by factors ranging from 0.4 to 0.04 relative to LiTFSI, depending on x and salt concentration. To our knowledge, this study represents the first systematic investigation of the effect of molecular structure of polymer electrolytes on polysulfide migration.

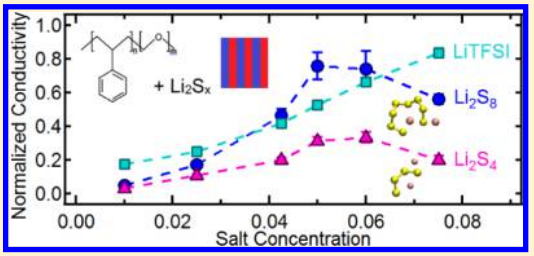

1. INTRODUCTION

There is considerable interest in rechargeable lithium−sulfur batteries because their theoretical specific energy, 2600 Wh/kg, is 5 times greater than that of current lithium-ion batteries.[1−3] Elemental sulfur is abundant, nontoxic, and inexpensive compared to cobalt- and iron-based cathodes in conventional lithium-ion batteries.[3] There are, however, many challenges that must be addressed before lithium−sulfur batteries become a commercial reality.[4] During the discharge of lithium−sulfur batteries, lithium polysulfide intermediates with chemical formulas Li_2S_x, where x ranges from 2 to 8, are formed. Some of these polysulfides dissolve in the electrolyte and diffuse out of the cathode.[5] Besides a permanent loss of active materials in the cathode, the dissolved Li_2S_x species participate in a parasitic shuttle between electrodes, resulting in capacity fade and self-discharge.[6] The reaction between polysulfides and active materials in the anode results in the formation of an insulating layer that increases cell resistance and compromises cycle life.[7] It is thus important to quantify diffusion and migration of lithium polysulfides in lithium battery electrolytes.

Recent work has focused on designing nanostructured cathodes that confine sulfur and polysulfides within the cathode without impeding transport of lithium ions and electrons, which are necessary for the redox reactions.[8−12] While these efforts have improved the cycle life of lithium−sulfur batteries, the diffusion of polysulfides out of the cathode has not been completely eliminated. It is conceivable that nanostructuring the electrolyte may be another approach for controlling the diffusion of polysulfides.

The theoretical specific energy of a battery with a sulfur cathode and a graphite anode is only 576 Wh/kg, a factor of 4 lower than that of a lithium−sulfur battery.[13] It is thus essential to have an electrolyte that is stable against lithium metal, as the lithium metal anode will be a necessary component of high specific energy batteries with sulfur cathodes. Dendrite formation on the lithium anode is a prominent failure mode in these batteries.[14−16] Previous work has shown that nanostructured block copolymer electrolytes, mixtures of polystyrene-*b*-poly(ethylene oxide) (SEO) and lithium bis(trifluoromethanesulfonyl)imide (LiTFSI), slow down the

Received: May 6, 2015
Revised: June 23, 2015
Published: July 6, 2015

DOI: 10.1021/acs.macromol.5b00928
Macromolecules 2015, 48, 4863−4873

dendrite growth in lithium metal batteries.[17−23] This approach was motivated by theoretical calculations by Monroe and Newman, who predicted that electrolytes with high shear moduli were needed to stabilize lithium metal anodes.[24] The glassy polystyrene microphases endow SEO electrolytes with high moduli while the poly(ethylene oxide) (PEO) microphases provide channels for ion transport.[17−23] Understanding the electrochemical properties of SEO electrolytes containing lithium polysulfides is essential for evaluating their potential use in lithium−sulfur batteries.

Since polysulfides are ionic in nature, they may also migrate under the influence of electric fields. The importance of polysulfide migration can only be assessed after measuring transport properties such as conductivity, transference number, etc.[25] A significant problem in obtaining such data is that lithium polysulfides cannot be isolated.[26] Thus, making mixtures of solvents and polysulfides is nontrivial. Furthermore, polysulfides can undergo numerous spontaneous reactions: e.g., disproportionation reactions such as $2S_x^{2-} \leftrightarrows S_{x+m}^{2-} + S_{x-m}^{2-}$.[27,28] In a study of polysulfide species dissolved in PEO and SEO, Wujcik et al. showed that at a particular sulfur concentration (0.44 g S/g PEO) only Li_2S_4 and Li_2S_8 exist as pure species. In contrast, Li_2S_2 undergoes a disproportionation reaction to form Li_2S and Li_2S_4. Similarly, Li_2S_6 undergoes a disproportionation reaction to form Li_2S_4 and Li_2S_8.[29] Interpreting conductivity measurements of SEO/Li_2S_2 and SEO/Li_2S_6 systems would be complicated due to the presence of more than one polysulfide anion species. Therefore, in this study we focus on SEO mixed with Li_2S_4 and Li_2S_8. Conductivity of these mixtures is compared with that of PEO/Li_2S_4 and PEO/Li_2S_8 mixtures to quantify the effect of nanostructuring on ion transport. In a practical lithium−sulfur battery, one would like to choose an electrolyte wherein the ion transport of the salt, such as LiTFSI, used in the electrolyte is much more rapid than that of the polysulfides. We therefore compare the conductivity of SEO/polysulfide and PEO/polysulfide mixtures with that of SEO/LiTFSI and PEO/LiTFSI. For simplicity, we refer to both Li_2S_x and LiTFSI as salts.

To our knowledge, there are limited published reports on the conductivity of polysulfide/solvent mixtures; Chang et al. reported the conductivity of Li_2S_8 in tetraglyme,[30] and Agostini et al. reported the conductivity of a ball-milled mixture of Li_2S_8 in a PEO-based electrolyte containing additional salt.[31]

2. EXPERIMENTAL SECTION

2.1. Materials. PEO homopolymer with a number-averaged molecular weight, M_n, of 100 kg/mol was obtained from Sigma-Aldrich. The polymer was purified by dissolution in dichloromethane and subsequent precipitation in hexane. The purification process was repeated three times. The polymer was then dried in a vacuum oven at 90 °C for 24 h. The SEO block copolymer was synthesized on a high-vacuum line via sequential anionic polymerization.[31] The number-averaged molecular weights of the polystyrene (PS) and PEO blocks were 47 and 45 kg/mol, respectively. Both PEO and SEO were dried under vacuum at 90 °C for 24 h in the antechamber of an argon (Ar) glovebox and then taken into the glovebox. Sulfur (S_8) and lithium sulfide (Li_2S) were received under Ar from Alfa Aesar, opened in an Ar-filled glovebox, and used as received.[29] LiTFSI salt was received in an air-free package from Novolyte, transferred into a vial inside of the Ar glovebox, and then dried at 120 °C under vacuum for 3 days before using.[32]

2.2. Sample Preparation. Five types of samples were made for this study: PEO/Li_2S_8, PEO/Li_2S_4, SEO/Li_2S_8, SEO/Li_2S_4, and SEO/LiTFSI, following procedures established in refs 29 and 32. The polysulfide samples were made by dissolving the polymer of interest in dimethylformamide (DMF) by mixing at 90 °C on a heating plate for 5 h. Separately, an Li_2S_x solution was made by mixing Li_2S and S_8 in DMF at 90 °C for 5 h in a sealed vial. The Li_2S to S_8 ratio was determined by the stoichiometric reaction

$$Li_2S + \frac{x-1}{8}S_8 \rightarrow Li_2S_x \quad (x = 4 \text{ or } 8)$$

The Li_2S_x/DMF solution and the polymer/DMF solution were then mixed together at 90 °C for 24 h in a sealed vial. The polymer/Li_2S_x samples were obtained by drying the mixed solutions in a Teflon Petri dish at 75 °C under Ar for 3 days, followed by drying at 50 °C under vacuum for 15 h. Removal of the solvent and retention of the polysulfides in the samples were confirmed using elemental analysis to determine the relative ratios of C, H, N, and S at the Microanalytical Laboratory in the College of Chemistry, University of California, Berkeley.

SEO/LiTFSI samples were prepared by dissolving the components separately in DMF and mixing the two solutions at 90 °C for 24 h. The mixed solutions were dried at 90 °C in an Ar environment for 24 h and then dried at 90 °C under vacuum in the glovebox antechamber for 24 h to get the sample.

In our previous studies, the concentration of lithium salts in PEO-containing polymers is defined as the molar ratio of lithium atoms to ethylene oxide moieties, $r = [Li^+]/[EO]$.[17−23,32] Whether or not the same definition should be used to describe PEO/Li_2S_x and SEO/Li_2S_x mixtures is an interesting open question. In most publications, lithium polysulfides are depicted as linear chains with charged sulfur and lithium ions at the chain ends.[33−35] Such depictions suggest that both lithium ions might, in principle, dissociate from the polysulfide chains. Simulations of polysulfides in PEO by Pascal et al. show a different molecular configuration, as shown in Figure 1. The S_4^{2-} and S_8^{2-} chains form a claw-like structure, with one Li^+ localized within the claw and the other outside of the claw.[36] It is thus likely that Li_2S_x molecules dissociate into LiS_x^- and Li^+. In this paper, we thus define our salt concentration, R, as

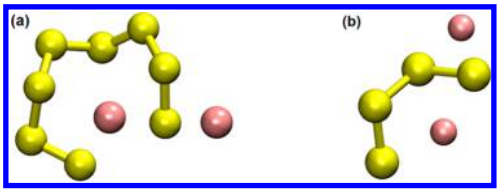

Figure 1. Typical simulation results of (a) Li_2S_8 and (b) Li_2S_4 configurations in a matrix of short PEO chains (matrix not shown for simplicity) taken from ref 36. The red spheres represent lithium ions.

$$R = \frac{[Li^+]}{|z^-|[EO]} \quad (1)$$

where $|z^-|$ is the magnitude of the charge of the anion. For Li_2S_x, $|z^-| = 2$, and for LiTFSI, $|z^-| = 1$. Given our current understanding, it is best, in our opinion, to compare polymer/Li_2S_x and polymer/LiTFSI mixtures with the same value of R.

2.3. Small-Angle X-ray Scattering (SAXS). The morphology of the polymer/Li_2S_x samples was determined by SAXS. Each sample was pressed into a 1 mm thick fiberglass reinforced silicone spacer with a diameter of 3.18 mm inside an Ar glovebox. Both ends of the spacer were sealed with Kapton windows in a custom-designed airtight sample holder. All samples were annealed at 120 °C under Ar for 24 h to eliminate any strain induced during sample preparation.

SAXS measurements were performed at beamline 7.3.3 at the Advanced Light Source (ALS) at Lawrence Berkeley National Laboratory using 10 keV monochromatic X-rays.[37] Samples were mounted in a custom-built heating stage, and the sample-to-detector distance and beam center were calibrated using a silver behenate

DOI: 10.1021/acs.macromol.5b00928
Macromolecules 2015, 48, 4863−4873

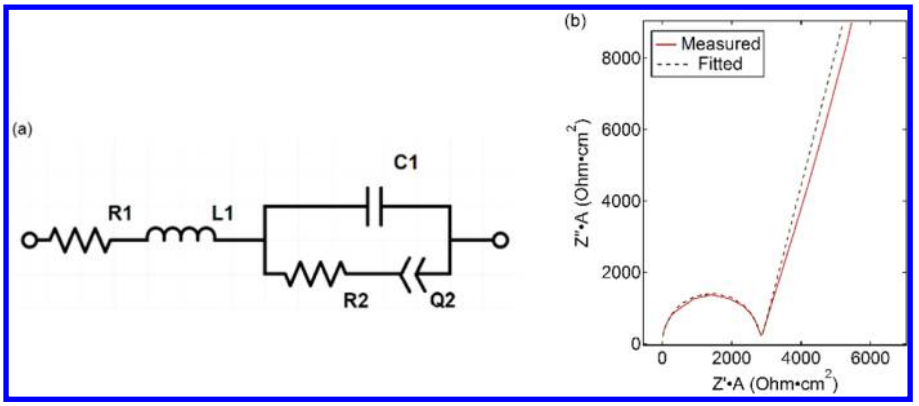

Figure 2. (a) Equivalent circuit for determining the ionic resistance of the polymer/salt electrolytes with blocking electrodes. (b) Typical experimental data plotted in the Nyquist format of SEO/Li_2S_4 at 70 °C (R = 0.025). The simulated impedance diagram is indicated by a dashed line.

standard. The samples were heated from 30 to 120 °C and cooled to 60 °C, with increments of 30 °C during heating and increments of 10 °C during cooling, before being cooled back to room temperature. The samples were held at each temperature for 30−60 min before taking the measurements. All images were obtained using 2 s exposures. The Nika macro for Igor Pro developed by Jan Ilavsky was used to reduce the two-dimensional SAXS patterns,[38] and the azimuthally averaged intensity, I, was plotted against the magnitude of the scattering vector, $q = 4\pi \sin(\theta/2)/\lambda$, where θ is the scattering angle and λ is the wavelength of the X-ray. Each scattering data was further processed by subtracting the background scattering from the blank, an empty sample cell, using eq 2:

$$I = I_{\text{sample}} - \frac{T_{\text{sample}}}{T_{\text{blank}}} \times I_{\text{blank}} \tag{2}$$

where I_{sample} and I_{blank} are the raw scattering intensities from the sample and the empty cell respectively, and T_{sample} and T_{blank} are transmission coefficients of the sample and the blank, respectively.

2.4. Differential Scanning Calorimetry (DSC). PEO/Li_2S_x and SEO/Li_2S_x samples were sealed in hermetic aluminum pans in an Ar glovebox for DSC experiments, which were performed on a Thermal Advantage 2920 instrument. All samples were heated to 150 °C at a rate of 10 °C/min, cooled to −70 °C at a rate of 5 °C/min, and heated again to 150 °C at a rate of 10 °C/min. Data from the second heating are presented in this paper.

2.5. AC Impedance Spectroscopy. The ionic conductivity of each sample was measured by ac impedance spectroscopy. Each sample was mechanically pressed into a 0.125 mm thick epoxy fiberglass, Garolite-10 spacer with a diameter of 4.76 mm. Two high purity, 19 μm thick aluminum electrode foils were pressed on each side of the polymer contained spacer. The area of the sample was determined by the size of the hole in the spacer, and the thickness of the sample was measured with a micrometer. Two aluminum tabs were attached to each of the electrode foils to make electrical contacts. The samples were then placed in a laminated aluminum pouching material and sealed under vacuum before removing them from the glovebox.

A Biologic VMP3 potentiostat was used to measure the real and imaginary impedances, Z' and Z'', of the samples using an ac signal with 80 mV amplitude and frequencies varying from 1 Hz to 1 MHz. The impedance spectrum was interpreted by an equivalent circuit shown in Figure 2a. The equivalent circuit is composed of R_2, the electrolyte resistance, in series with Q_2, the blocking electrode/electrolyte interfaces pseudocapacitance, together in parallel with C_1, the geometrical capacitance due to the finite dielectric constant of the electrolyte between the two parallel metallic electrodes, and together in series with the apparatus resistance, R_1, and the inductance, L_1.[39,40] The impedance locus simulated by using this equivalent circuit is used to determine R_2, the resistance due to ion transport in the electrolyte.

The conductivity of the electrolyte is determined by eq 3:

$$\sigma = \frac{l}{R_2 A} \tag{3}$$

where l is the sample thickness, which is remeasured after the measurements, and A is the area. The conductivity of salt-containing samples is reported after subtracting the measured conductivities of pure PEO and SEO. Values for conductivities of pure polymers range between 1.91 × 10^{-7} and 5.33 × 10^{-7} S/cm. Three independent replicates at each salt concentration were used to determine the conductivity of SEO/Li_2S_x and PEO/Li_2S_x samples. Only one sample at a given salt concentration was used to determine the conductivity of SEO/LiTFSI samples.

2.6. X-ray Absorption Spectroscopy (XAS). Thin film samples for concentration-dependent XAS experiments were prepared by spin-coating solutions of PEO containing Li_2S_8 and Li_2S_4 in DMF as described in our previous study.[29] The samples for each "x" value were prepared from one single bulk solution (e.g., Li_2S_8 at a concentration of 0.2 g S/g PEO was prepared from the same Li_2S_8/DMF solution as the 0.5 g S/g PEO). The range of R values covered are 0.034−0.086 for Li_2S_8 and 0.069−0.172 for Li_2S_4. This means that the observed spectra only reflect the different salt concentrations and not small differences in "x" values. The experimental Li_2S_x "x" values were 7.97 and 4.01 for the Li_2S_8 and Li_2S_4 solutions, respectively. The PEO used to make the thin film samples had a molecular weight of 55 kg/mol (Polymer Source Inc.). Samples were spin-coated at 2000 rpm for 60 s, at room temperature, with 30 μL of solution.

Thin film samples are not appropriate for temperature studies due to the potential of sulfur loss during measurements. We thus conduct these measurements on liquid samples. Polysulfide solutions were prepared by mixing Li_2S and S_8 in PEO at 90 °C for 3 days. The molecular weight of the PEO was 600 g/mol and was obtained from Polymer Source Inc. The experimental Li_2S_x "x" value for the Li_2S_8 solution was 7.97, and that of the Li_2S_4 solution was 4.00. The concentration of polysulfide species in the Li_2S_8 sample corresponded to R = 0.005, and the concentration of the Li_2S_4 sample corresponded to R = 0.015. These low salt concentrations were used to avoid X-ray overabsorption. After 3 days of mixing, solutions were brought to the Stanford Synchrotron Radiation Lightsource (SSRL) and placed in an Ar glovebox. Prior to measurement, approximately 0.3 mL of each solution was loaded into an airtight, custom-made liquid cell containing a 3 μm thin film of Mylar that served as an X-ray transparent window.

Unfortunately, due to instrumental limitations, the concentration and temperature range over which XAS experiments were performed are different from those used in our morphology and conductivity studies. Entirely different XAS setups would be needed to cover the concentrations used in our morphology and conductivity studies.

XAS experiments were performed at beamline 4-3 at SSRL. Samples were measured in fluorescence mode using a four-element silicon Vortex detector. The beamline energy was calibrated using sodium thiosulfate, setting the first centroid peak to 2472.02 eV. Spectra were

DOI: 10.1021/acs.macromol.5b00928
Macromolecules 2015, 48, 4863−4873

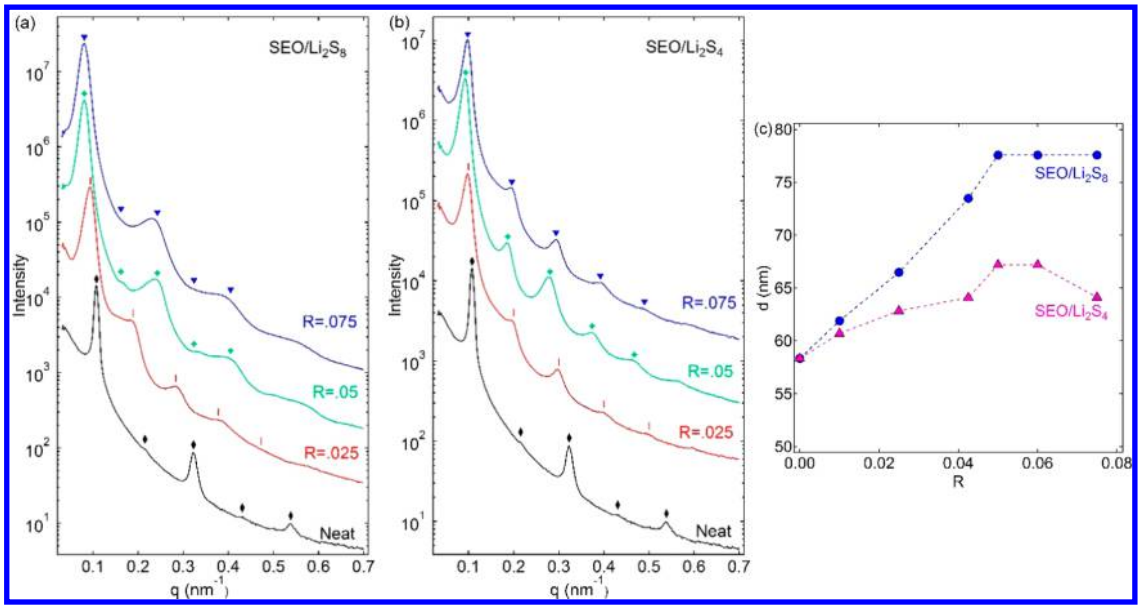

Figure 3. SAXS intensity versus magnitude of the scattering vector, q, for (a) SEO/Li_2S_8 and (b) SEO/Li_2S_4 at 90 °C. Profiles are offset for clarity. Markers on top of each profile indicate the expected locations for q^*, $2q^*$, $3q^*$, $4q^*$, and $5q^*$. (c) Lamellar domain spacing, d, versus the Li_2S_x concentration, R.

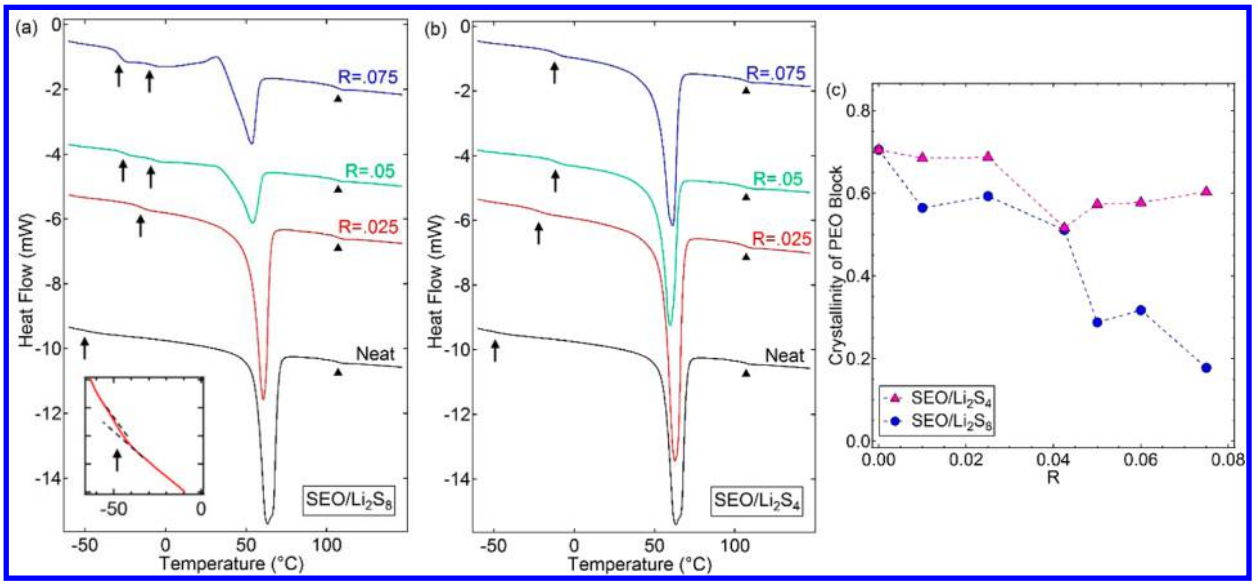

Figure 4. DSC scans of (a) SEO/Li_2S_8 and (b) SEO/Li_2S_4. Scans are offset for clarity. Inset in (a) shows the DSC scan of neat PEO on an expanded scale. Arrows show T_g^{PEO} and triangles show T_g^{PS}. (c) Effect of salt concentration, R, on the crystallinity of the PEO microphase for SEO/Li_2S_x samples.

taken over the range of 2440−2575 eV with an energy resolution as low as 0.08 eV near the absorption edge. Three consecutive scans were taken for each sample, and at each temperature, without any movement of the sample stage between scans and then averaged for further data analysis. Samples were allowed to rest for 20 min after each change in temperature to allow for full equilibration. X-ray spectra were normalized and background subtracted using SIXPACK.

3. RESULTS AND DISCUSSION

3.1. Morphology. We first examine the morphology of SEO/Li_2S_x mixtures. Figures 3a and 3b show selected SAXS profiles of the block copolymer with Li_2S_8 and Li_2S_4, respectively, over a range of salt concentrations, R = 0−0.075. All of the SAXS profiles in Figure 3 are consistent with a lamellar morphology. The center-to-center distance between adjacent PS lamellae, d, is given by $2\pi/q^*$, where q^* is the value of q at the primary peak. Higher order peaks at $2q^*$, $3q^*$, $4q^*$, and $5q^*$ are evident in most samples. The even order peaks are absent in the R = 0 sample due to the minima in the form factor of lamellae. The dependence of d on R is shown in Figure 3c. For SEO/Li_2S_8 samples, d increases more or less linearly with R for values less than 0.05 from 58 to 78 nm, approaching a plateau for higher values of R. In contrast, for SEO/Li_2S_4 samples, d is a nonmonotonic function of R, with a shallow maximum at R between 0.05 and 0.06, as shown in Figure 3c. We are not sure of the reason for the slight decrease in d with increasing R at R > 0.06. The domain spacing at fixed R is higher for SEO/Li_2S_8 samples compared to SEO/Li_2S_4 samples. The SAXS profiles of SEO/Li_2S_x mixtures were insensitive to

DOI: 10.1021/acs.macromol.5b00928
Macromolecules 2015, 48, 4863−4873

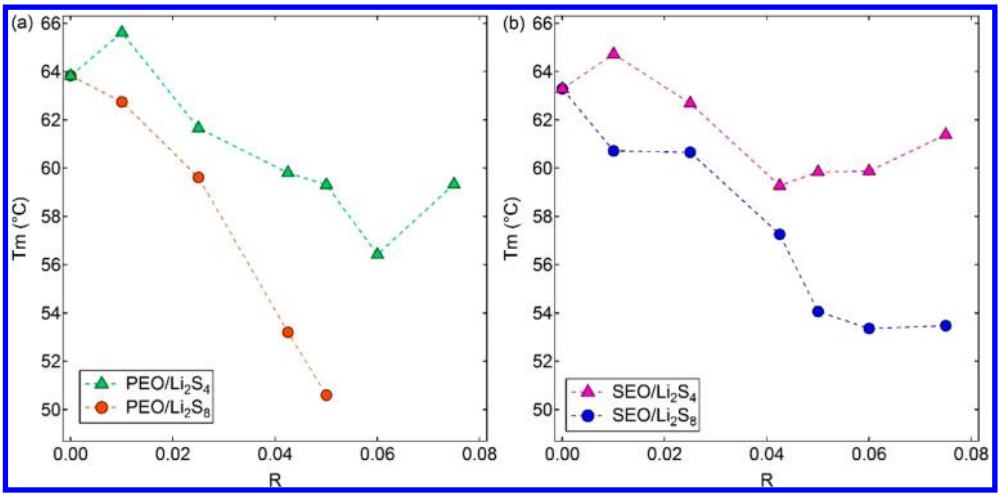

Figure 5. Melting temperature of PEO, T_m, versus salt concentration, R, for (a) PEO/Li_2S_x samples and (b) SEO/Li_2S_x samples.

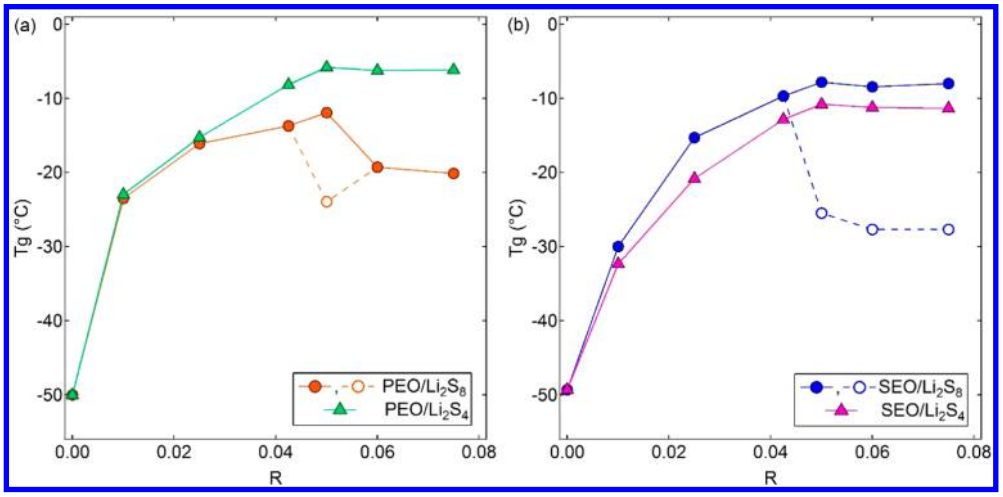

Figure 6. Glass transition temperature of PEO, T_g^{PEO}, versus salt concentration, R, for (a) PEO/Li_2S_x samples and (b) SEO/Li_2S_x samples.

changes in temperature; the maximum change in d over the temperature range from 60 to 120 °C was 1.6%.

3.2. Thermal Properties. Figures 4a and 4b show DSC scans for selected concentrations of SEO/Li_2S_8 and SEO/Li_2S_4, respectively. The enthalpy of melting of the PEO crystals in our samples, ΔH_m, is related to the area under the melting peak seeing in Figure 4. ΔH_m generally decreases with increasing salt concentration in both samples. As R increases from 0 to 0.075, ΔH_m decreases from 64 to 14 J/g in SEO/Li_2S_8 and from 64 to 46 J/g in SEO/Li_2S_4. The degree of crystallinity was calculated according to eq 4

$$\text{crystallinity} = \frac{\Delta H_m}{\omega_{EO}\Delta H_m^0} \quad (4)$$

where ω_{EO} is the weight fraction of ethylene oxide (EO) in each sample, ΔH_m is the melting enthalpy of the sample, which is evaluated by integrating the area under the melting endothermic peak in the second heating scan, and ΔH_m^0 is the melting enthalpy of 100% crystalline PEO. Literature value for ΔH_m^0 ranges from 134 to 214 J/g.[41−47] Here, for concreteness, we use a value of 186 J/g for ΔH_m^0. The effect of Li_2S_8 and Li_2S_4 concentrations on the crystallinity of the PEO/Li_2S_x microphase in SEO/Li_2S_x samples is shown in Figure 4c. The polarity of ether oxygen atoms on PEO backbones and the suitable distance between them enables coordination of lithium ions,[48] causing lithium salts to segregate into PEO microphases. This suppresses crystallization of PEO chains, and crystallinity generally decreases with increasing salt concentrations in both SEO/Li_2S_8 and SEO/Li_2S_4 samples. The suppression of crystallinity in SEO/Li_2S_4 samples is less significant than that in the SEO/Li_2S_8 samples, indicating that PEO/Li_2S_8 interactions are more favorable than PEO/Li_2S_4 interactions.

Figure 5a plots the measured melting temperature of crystalline PEO, T_m, of PEO/Li_2S_8 and PEO/Li_2S_4 samples obtained from the DSC scans shown in Figure S1 in the Supporting Information. In the PEO/Li_2S_8 samples, T_m decreases monotonically from 64 to 51 °C as R increases from 0 to 0.05. We do not see a melting peak for R > 0.05, indicating that the crystallinity of PEO is completely suppressed in high Li_2S_8 concentration samples. In the range R = 0−0.075, T_m of PEO/Li_2S_4 samples range from 56 to 66 °C. Figure 5b shows T_m of SEO/Li_2S_8 and SEO/Li_2S_4 samples obtained from the DSC scans shown in Figure 4. In the SEO/Li_2S_8 samples, T_m monotonically decreases from 63 to 54 °C as R increases from 0 to 0.05 and reaches a plateau for R > 0.05. In the range R = 0−0.075, T_m of SEO/Li_2S_4 samples range from 65 to 59 °C. Reproducibility of measured T_m values is about 1 °C. It is clear that T_m is a weak function of salt concentration in both

DOI: 10.1021/acs.macromol.5b00928
Macromolecules 2015, 48, 4863−4873

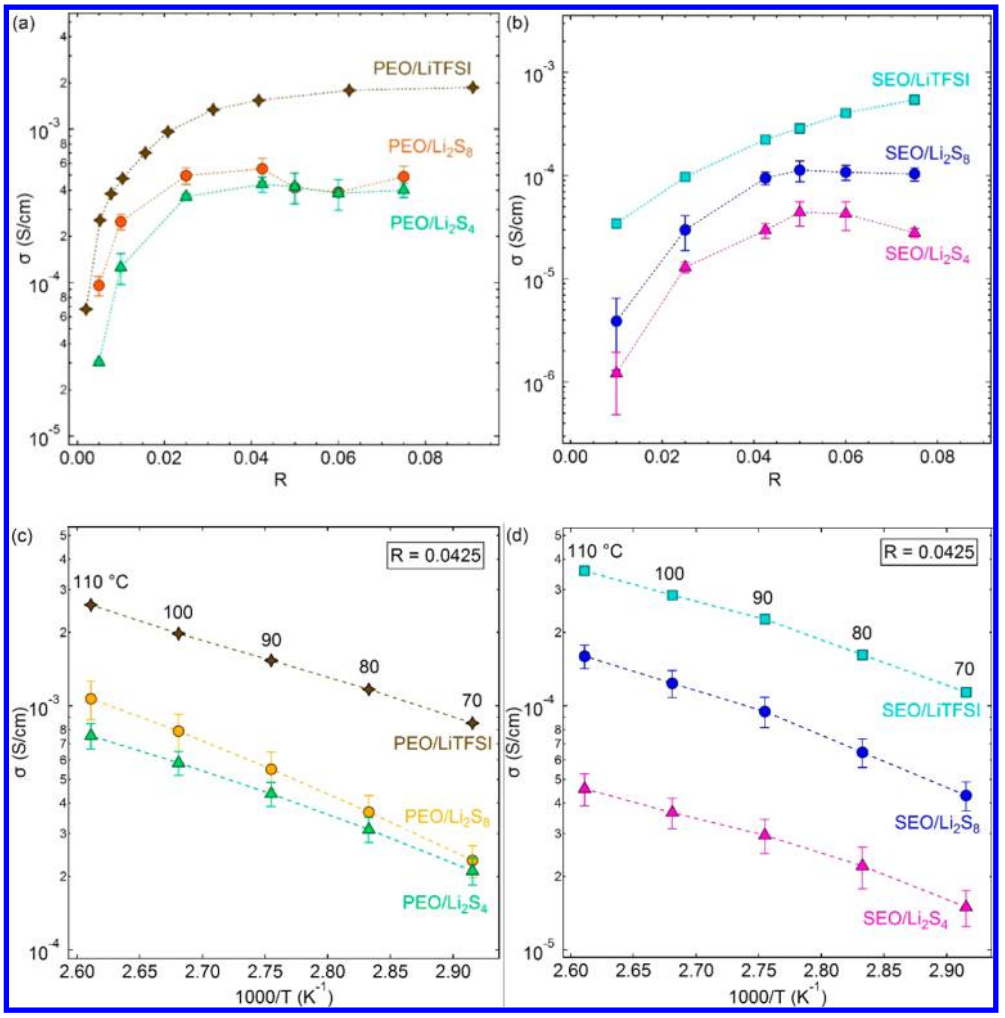

Figure 7. Conductivity, σ, versus salt concentration, R, for (a) PEO/salt samples and (b) SEO/salt samples at 90 °C. Conductivity, σ, versus inverse temperature, 1000/T, for (c) PEO/salt samples and (d) SEO/salt samples at R = 0.0425.

PEO/Li_2S_4 and SEO/Li_2S_4 samples. The T_m values of both PEO/Li_2S_4 and SEO/Li_2S_4 samples with R = 0.01 are slightly higher than those of the neat polymers. We do not know the reason for this observation.

The DSC scans of SEO/Li_2S_8 and SEO/Li_2S_4 show glass transition temperatures below 0 °C and above 100 °C. The former corresponds to the glass transition of the PEO-rich microphase while the latter corresponds to the glass transition of the PS-rich microphase. The DSC scans of PEO/Li_2S_8 and PEO/Li_2S_4, shown in Figure S1 of the Supporting Information, only show glass transitions below 0 °C. Figure 6a plots the measured glass transition temperature, T_g^{PEO}, of PEO/Li_2S_8 and PEO/Li_2S_4 samples. In the low salt concentration limit PEO/Li_2S_8 samples exhibit a single glass transition; T_g^{PEO} increases from −50 to −14 °C as R increases from 0 to 0.0425. At R = 0.05, two glass transitions are observed. This can be seen if one carefully examines the DSC scan in Figure S1a. To clarify this phenomenon, expanded views of the DSC scans at R = 0.0425 and 0.05 are shown in Figure S2 of the Supporting Information. A single glass transition is clearly obtained at R = 0.0425 while two glass transitions at −24 and −12 °C are obtained at R = 0.05. A single T_g^{PEO} is recovered upon increasing R to 0.06 and beyond as shown in Figure 6a. All PEO/Li_2S_4 samples exhibit a single T_g which increases from −50 to −6 °C as R increases from 0 to 0.05 and reaches a plateau for R > 0.05. Figure 6b shows T_g^{PEO} of SEO/Li_2S_8 and SEO/Li_2S_4 samples obtained from the DSC scans shown in Figure 4. In the SEO/Li_2S_8 samples, T_g^{PEO} increases from −49 to −10 °C as R increases from 0 to 0.0425. For $R \geq 0.05$, two T_g^{PEO} values are observed: a higher T_g^{PEO} value at −8.1 ± 0.4 °C and a lower T_g^{PEO} value at −26.1 ± 1.6 °C. The dependence of T_g^{PEO} on R in the SEO/Li_2S_4 samples is similar to that in the PEO/Li_2S_4 samples; T_g^{PEO} increases from −49 to −11 °C as R increases from 0 to 0.05 and reaches a plateau for R > 0.05.

The presence of two glass transitions in both PEO/Li_2S_8 and SEO/Li_2S_8 samples appears to be related to both salt concentration and crystallinity. In dilute samples with $R \leq$ 0.0425, a single T_g^{PEO} is obtained in both systems (Figure 6). Increasing R to 0.05 results in two glass transitions in PEO/Li_2S_8 and SEO/Li_2S_8. These samples are semicrystalline in the vicinity of their glass transition temperatures. It is reasonable to assume that salt molecules are localized in the amorphous portions of PEO. We propose that two glass transitions reflect two different amorphous regions: one with high salt concentration and the other with low salt concentration. The heterogeneity in salt distribution disappears when crystallinity is lost as is the case in PEO/Li_2S_8 at R = 0.06 and beyond. Further work is needed to determine the underpinnings of the observed behavior of glassy and semicrystalline PEO-rich microphases containing Li_2S_x. The main focus of this work is to quantify ion

DOI: 10.1021/acs.macromol.5b00928
Macromolecules 2015, 48, 4863−4873

transport at temperatures above the melting temperature of PEO. Our limited understanding of salt distribution in crystalline samples does not affect interpretation of ion transport data given below.

The glass transition temperature of the PS microphase, T_g^{PS}, in the SEO/Li_2S_x samples at all salt concentrations are at 107 ± 1 °C. The insensitivity of T_g^{PS} of PS microphase with salt concentration indicates that Li_2S_x molecules do not interact with PS.

3.3. Electrochemical Properties. Our electrochemical characterization experiments are limited to temperatures above the melting temperature of PEO. Figure 7a plots the measured conductivity of PEO/Li_2S_8 and PEO/Li_2S_4 samples at 90 °C. Also shown in Figure 7a is the conductivity of PEO/LiTFSI, taken from the work of Lascaud et al.[49] The conductivity of PEO/Li_2S_x increases rapidly at low R values, and reaches a plateau at R = 0.0425. The conductivity of PEO/Li_2S_8 is higher than that of the PEO/Li_2S_4 samples at R < 0.05 and becomes similar at $R \geq 0.05$. Within this concentration range, the conductivity of PEO/LiTFSI increases monotonically with salt concentration. (The conductivity of PEO/LiTFSI measured by Lascaud et al. peaks at R = 0.085 and decreases slowly until R = 0.5.) The conductivity of mixtures containing Li_2S_x are generally lower than that of mixtures containing LiTFSI. At high salt concentrations (R > 0.04), the conductivity of Li_2S_x mixtures is about a factor of 5 lower than that of LiTFSI mixtures.

Figure 7b shows the conductivity of SEO/Li_2S_8 and SEO/Li_2S_4 samples. Also shown in Figure 7b is the conductivity of SEO/LiTFSI. The trends seen in Figure 5b can be anticipated from the PEO data in Figure 5a. The conductivity versus R curves of SEO/Li_2S_8 and SEO/Li_2S_4 are nearly parallel to each other; the conductivity of SEO/Li_2S_8 is about a factor of 2 higher than that of SEO/Li_2S_4 at all salt concentrations. The conductivity of SEO/LiTFSI is higher than that of both polysulfide mixtures at all concentrations. The conductivity of SEO/Li_2S_4 mixtures at R > 0.05 is a weak function of salt concentration. It is well-known that increasing the glass transition temperature lowers the conductivity of polymer electrolytes.[40,48] The glass transition temperature of our PEO/Li_2S_x, and that of the PEO microphase in SEO/Li_2S_x, T_g^{PEO}, increases with increasing R (Figure 6). The increase in conductivity with increasing R (Figures 7a and 7b) might have been larger if T_g^{PEO} were unaffected by R. Figures 7c and 7d show the conductivity of PEO/salt and SEO/salt, respectively, at R = 0.0425. All conductivities increase with temperature.

In Figure 8, we plot σ as a function of d for SEO/Li_2S_8 and SEO/Li_2S_4 at 90 °C. Both sets of data appear to collapse onto a single curve, suggesting a relationship between transport and thermodynamics; the values of d reflect thermodynamic interactions between polysulfides and PEO chains.

The effect of morphology on conductivity of block copolymer/salt mixtures can be quantified by examining normalized conductivities. The normalized conductivity, σ_n, is defined by eq 5

$$\sigma_n = \frac{\sigma_{SEO/salt}}{f\varphi_{EO/salt}\sigma_{PEO/salt}} \quad (5)$$

where $\sigma_{SEO/salt}$ and $\sigma_{PEO/salt}$ are conductivities of the two systems at the same value of R, $\phi_{EO/salt}$ is the volume fraction of the PEO/salt microdomains, and f is the morphology factor

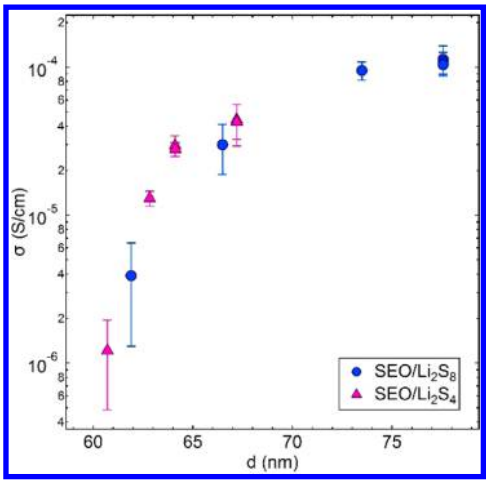

Figure 8. Conductivity, σ, versus domain spacing, d, for SEO/Li_2S_x samples at 90 °C.

that accounts for the geometry of the conducting microdomains. Since all of the SEO/salt mixtures have a lamellae morphology, f = 2/3.[22]

In Figure 9 we plot σ_n versus T of SEO/LiTFSI, SEO/Li_2S_8, and SEO/Li_2S_4 samples in the temperature range 70−110 °C. The normalized conductivity of SEO/LiTFSI increases with increasing temperature, while the normalized conductivities of SEO/Li_2S_8 and SEO/Li_2S_4 decrease with increasing temperature. The SEO/salt data indicate a slight suppression of migration of Li_2S_x species in SEO compared to PEO with increasing temperature. If the proposed normalization scheme accurately described transport of salt through block copolymers, then σ_n would be independent of temperature. The finite slopes of linear fits through the data in Figure 9 indicate limitations in the proposed normalization scheme. We quantify this by fitting the data in Figure 9 to the linear equation

$$\sigma_n = \sigma_n^\circ\left[1 + m\frac{T - 90}{40}\right] \quad (6)$$

where σ_n° is the fitted value of σ_n of each sample at a reference temperature of 90 °C ($\sigma_n^\circ = a + 90b$, where a and b are intercepts and the slope of the fitted line, respectively, as shown in Figure 9a−c). The parameter m signifies the relative change of σ_n in the temperature range of interest. The plot of m versus R in Figure 10 shows that the magnitude of m averages around 0.2. We do not know the reason for the observed slight suppression of polysulfide migration as a function of increasing temperature. In the discussion below, we present the temperature-averaged values of σ_n.

Figure 11 shows the temperature-averaged normalized conductivities, σ_n, for all three salts. The σ_n for LiTFSI samples increases monotonically over the measured concentration range, while the σ_n for both Li_2S_8 and Li_2S_4 samples increases initially with salt concentration, peaks between R = 0.05 and R = 0.06 and decreases at higher concentrations. The σ_n for Li_2S_4 is lower than that of Li_2S_8 at all salt concentrations, indicating that SEO hinders the migration of Li_2S_4 more significantly than it hinders the migration of Li_2S_8. This effect is more prominent at higher salt concentrations.

In Li−S battery applications, one is interested in suppressing migration of polysulfides without interfering with the migration of the electrolyte salt. It is therefore instructive to examine σ_R defined as the ratio of conductivity of the polymer of interest

DOI: 10.1021/acs.macromol.5b00928
Macromolecules 2015, 48, 4863−4873

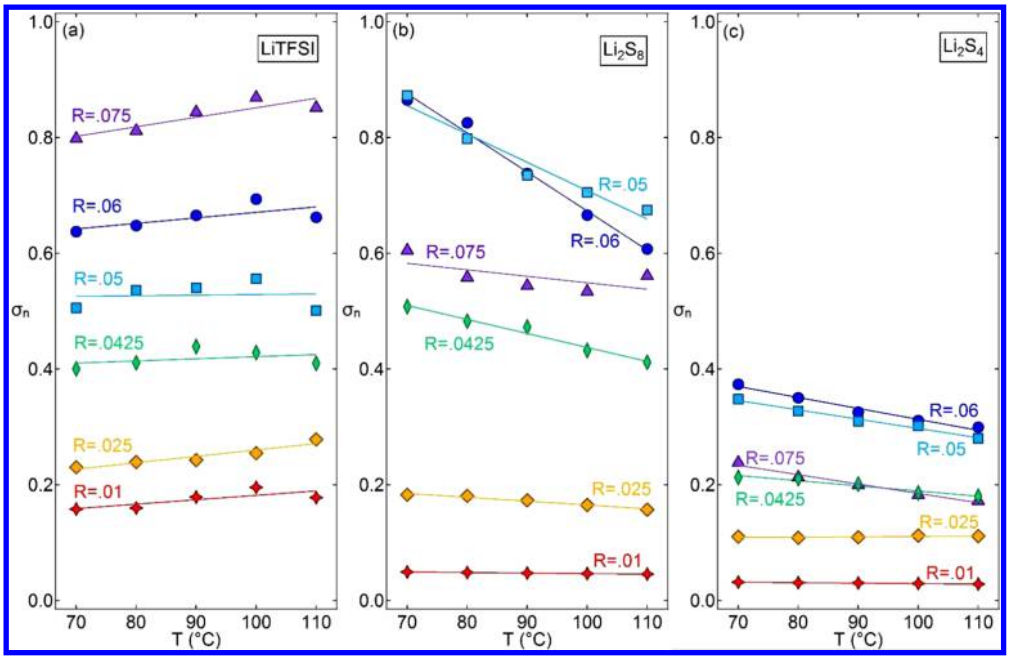

Figure 9. Normalized conductivity, σ_n, of (a) SEO/LiTFSI, (b) SEO/Li_2S_8, and (c) SEO/Li_2S_4 versus temperature, T.

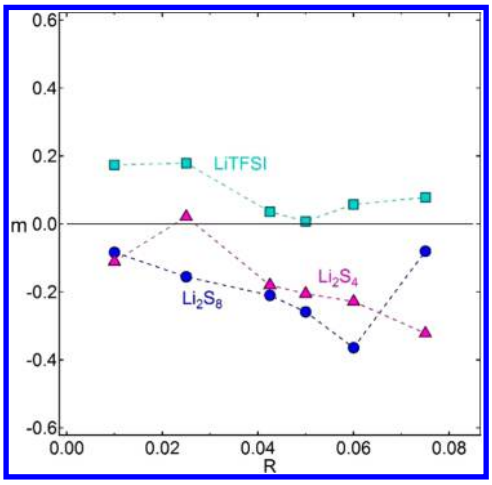

Figure 10. Plot of m versus salt concentration, R. The parameter m is a nondimensional measure of the temperature dependence σ_n as defined in eq 6.

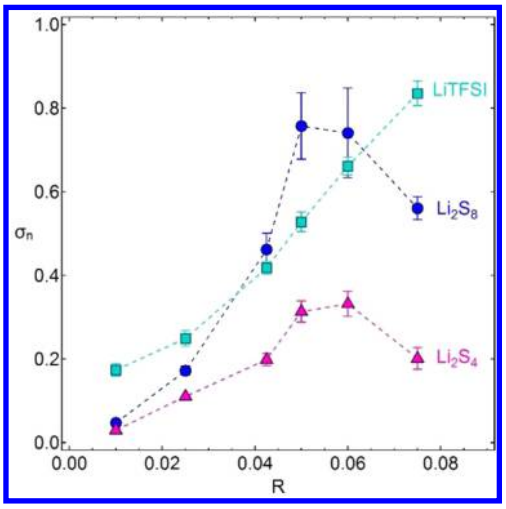

Figure 11. Temperature-averaged normalized conductivity, σ_n, versus salt concentration, R. The error bars represent the standard deviation of σ_n.

containing Li_2S_x to the conductivity of the same polymer containing LiTFSI at the same value of R.

$$\sigma_R = \frac{\sigma_{polymer/Li_2S_x}}{\sigma_{polymer/LiTFSI}} \quad (7)$$

Suppression of Li_2S_8 migration due to the nanostructured nature of SEO is only seen at low salt concentrations; σ_R of SEO is less than that of PEO when $R < 0.04$ (Figure 12a). At higher salt concentrations, σ_R of Li_2S_8 in SEO and in PEO are comparable, indicating no suppression due to the presence of a nanostructured electrolyte. In contrast, Li_2S_4 migration in SEO is significantly suppressed compared to that in PEO (Figure 12b); σ_R of SEO is less than that of PEO over the entire concentration range. The σ_R versus R curves of SEO/Li_2S_x appeared to be peaked in the vicinity of $R = 0.04$, while those of PEO/Li_2S_x are peaked at significantly lower salt concentrations.

The data in Figures 7−12 indicate that Li_2S_x species dissociate in both PEO and SEO to generate carrier ions that contribute to ionic conductivity, and their conductivities are somewhat lower than those of LiTFSI in both PEO and SEO. More importantly, Li_2S_x migration can be partially suppressed by SEO but cannot be prevented. However, since the diffusion coefficients and the cation transference numbers for polymer/Li_2S_x samples have not yet been measured, it is not clear whether the suppression is due to a reduction in carrier concentration or a reduction in mobility.[25]

In Figure 13, we show XAS spectra obtained from PEO/Li_2S_8 and PEO/Li_2S_4 mixtures at a variety of temperatures and salt concentrations. The spectra of Li_2S_8 and Li_2S_4 do not depend on either temperature or salt concentration. We therefore conclude that these species are maintained over the salt concentration and temperature ranges used in these experiments. While we cannot make concrete conclusions about the nature of the polysulfide mixtures used in our study of morphology and conductivity, the data in Figure 13 suggest

DOI: 10.1021/acs.macromol.5b00928
Macromolecules 2015, 48, 4863−4873

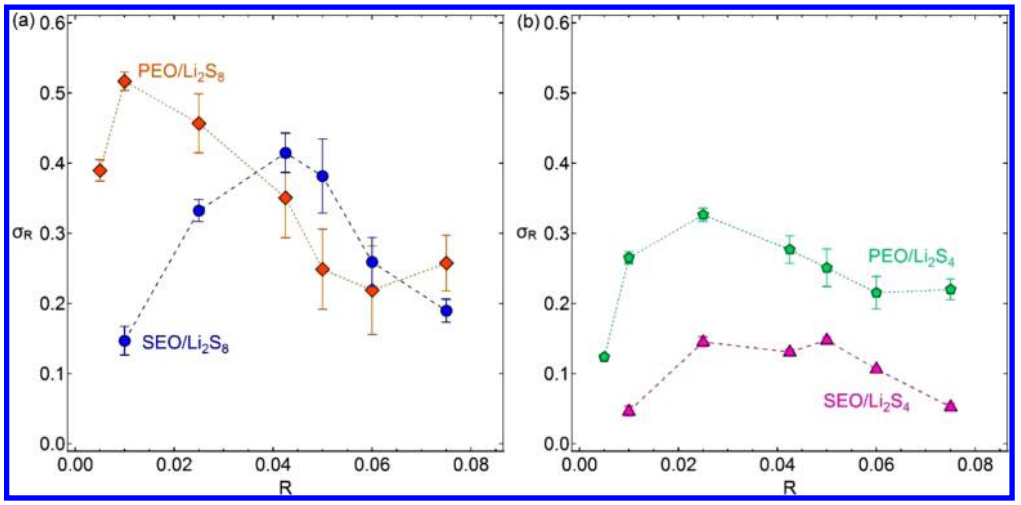

Figure 12. (a) Temperature-averaged ratio of polymer/Li_2S_8 conductivity to polymer/LiTFSI conductivity, σ_R, versus salt concentration, R, and (b) temperature-averaged ratio of polymer/Li_2S_8 conductivity to polymer/LiTFSI conductivity, σ_R, versus salt concentration, R.

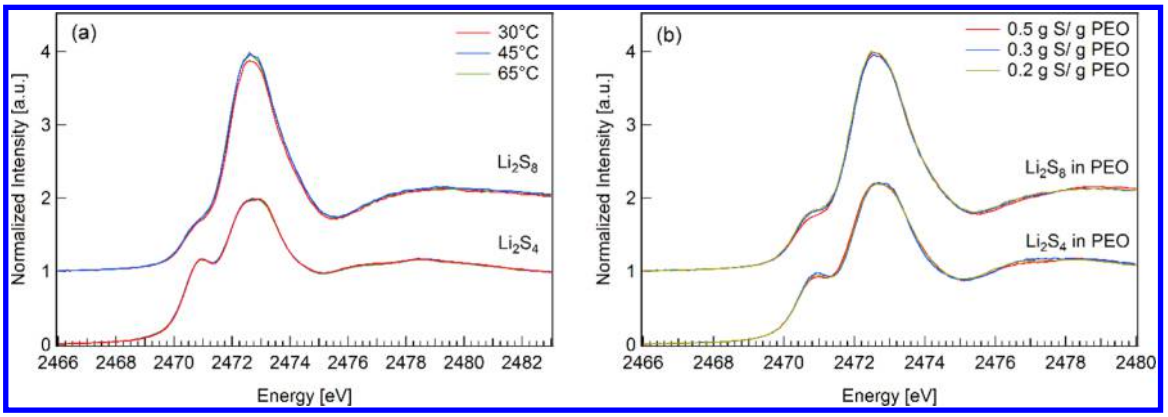

Figure 13. XAS sulfur K-edge spectra of Li_2S_4 and Li_2S_8 in PEO at (a) temperatures of 30, 45, and 65 °C and (b) sulfur concentrations of 0.2, 0.3, and 0.5 g of S per g of PEO. The overlapping spectra suggests no changes in polysulfide speciation as temperature and salt concentration is changed. The range of R values covered are 0.034−0.086 for Li_2S_8 and 0.069−0.172 for Li_2S_8.

that Li_2S_8 and Li_2S_4 are likely to remain intact over the temperature and salt concentration range of interest. In ref 29 it was shown that XAS spectra of Li_2S_x (x = 2−8) in SEO and PEO were identical. We thus do not expect the presence of the polystyrene block to affect speciation in SEO.

4. CONCLUSIONS

The morphology and the thermal properties of a polystyrene-*b*-poly(ethylene oxide) (SEO) block copolymer containing lithium polysulfides (Li_2S_x; x = 4, 8) were studied using small-angle X-ray scattering and differential scanning calorimetry. Both SEO/Li_2S_8 and SEO/Li_2S_4 samples showed a lamellar morphology at all concentrations. The crystallinity of the PEO lamellae was suppressed due to the presence of Li_2S_x, and this suppression was more significant in the case of SEO/Li_2S_8 samples relative to SEO/Li_2S_4 samples, suggesting that the interactions between PEO and Li_2S_8 are more favorable.

The conductivities of SEO/Li_2S_x and PEO/Li_2S_x samples were measured by ac impedance spectroscopy. The conductivities of both SEO and PEO samples containing Li_2S_8 are higher than the same polymer containing Li_2S_4 at all salt concentrations, indicating that dissociation of Li_2S_8 occurs more readily than Li_2S_4. We used normalized conductivity, σ_n, to focus on the effect of morphology on ion transport. Using this analysis, we show that SEO suppresses the migration of polysulfides relative to PEO.

Our study was motivated by the possibility of using nanostructured block copolymer electrolytes to suppress polysulfide migration in Li−S batteries. To examine this possibility, we evaluated σ_R, the ratio of the conductivity of SEO/Li_2S_x mixtures to that of SEO/LiTFSI mixtures; LiTFSI is a salt that is commonly used in batteries with PEO-based electrolytes. The values of σ_R range from 0.1 to 0.4 in the case of Li_2S_8 and from 0.04 to 0.15 in the case of Li_2S_4. This suppression is inadequate for practical applications. In other words, cathode architectures that prevent polysulfides from entering the electrolyte are necessary for enabling Li−S batteries with block copolymer electrolytes. Nevertheless, the results obtained in this study are important as they enable quantification of polysulfide migration in Li−S batteries with imperfect polysulfide encapsulation, a limitation that applies to all known Li−S batteries. To our knowledge, our work represents the first systematic investigation of the effect of molecular structure of polymer electrolytes on polysulfide migration.

DOI: 10.1021/acs.macromol.5b00928
Macromolecules 2015, 48, 4863−4873

■ ASSOCIATED CONTENT

Supporting Information

DSC scans of PEO/Li_2S_x systems. The Supporting Information is available free of charge on the ACS Publications website at DOI: 10.1021/acs.macromol.5b00928.

■ AUTHOR INFORMATION

Corresponding Author

*E-mail nbalsara@berkeley.edu (N.P.B.).

Notes

The authors declare no competing financial interest.

■ ACKNOWLEDGMENTS

This work was supported by the Office of Science, Office of Basic Energy Science, U.S. Department of Energy, under Contract DE-AC02-05CH11231 under the Soft Matter Electron Microscopy Program. SAXS measurements were carried out at the Advanced Light Source (Lawrence Berkeley National Lab), beamline 7.3.3, supported by the Office of Science, Office of Basic Energy Science, U.S. Department of Energy, under Contract DE-AC02-05CH11231. XAS experiments were carried out at the Stanford Synchrotron Radiation Lightsource, SLAC National Accelerator Laboratory, supported by the U.S. Department of Energy, Office of Science, Office of Basic Energy Sciences, under Contract DE-AC02-76SF00515. Elemental analysis is supported by the Microanalytical Laboratory of UC Berkeley, College of Chemistry. The authors gratefully acknowledge Tod Pascal and David Prendergast for providing the simulation results in Figure 1, Elena Kreimer for her assistance in elemental analysis, and Chenhui Zhu of the Advanced Light Source for his help with the X-ray scattering experiments.

■ ABBREVIATIONS

d, domain spacing (nm); f, morphology factor; m, relative change of σ_n per degree of change in T; q, scattering vector magnitude (nm^{-1}); r, molar ratio of lithium ions [Li^+] to ethylene oxide monomers [EO]; R, salt concentration: R = [Li^+]/($|z^-|$*[EO]); T, temperature (°C); T_g^{PEO}, glass transition temperature of PEO (°C); T_g^{PS}, glass transition temperature of PS (°C); T_m, melting temperature (°C); z^-, charge of anion species in salt molecules; ΔH_m, ΔH_m^0, heat of fusion (J/g); σ, ionic conductivity (S cm^{-1}); $\sigma_{SEO/salt}$, SEO/salt mixture ionic conductivity (S cm^{-1}); $\sigma_{PEO/salt}$, PEO/salt mixture ionic conductivity (S cm^{-1}); $\sigma_{polymer/Li_2S_x}$, polymer/Li_2S_x mixture ionic conductivity (S cm^{-1}); $\sigma_{polymer/LiTFSI}$, polymer/LiTFSI mixture ionic conductivity (S cm^{-1}); σ_n, temperature-averaged normalized ionic conductivity; σ_n°, linearly fitted value of σ_n at 90 °C; σ_R, ratio of $\sigma_{polymer/Li_2S_x}$ to $\sigma_{polymer/LiTFSI}$; $\Phi_{EO/salt}$, volume fraction of the PEO/salt block; ω_{EO}, weight fraction of ethylene oxide.

■ REFERENCES

(1) Rauh, R. D.; Abraham, K. M.; Pearson, G. F.; Surprenant, J. K.; Brummer, S. B. *J. Electrochem. Soc.* **1979**, *126*, 523−527.
(2) Brummer, S. B.; Rauh, R. D.; Marston, J. M.; Shuker, F. S. *Low Temperature Lithium/Sulfur Secondary Battery*; Energy Research and Development Administration, US Department of Energy: Washington, DC, 1976; pp 1− 57.
(3) Yamin, H.; Gorenshtein, A.; Penciner, J.; Sternberg, Y.; Peled, E. *J. Electrochem. Soc.* **1988**, *135*, 1045−1048.
(4) Kolosnitsyn, V. S.; Karaseva, E. V. *Russ. J. Electrochem. Soc.* **2008**, *44*, 506−509.
(5) Akridge, J. R.; Mikhaylik, Y. V.; White, N. *Solid State Ionics* **2004**, *175*, 243−245.
(6) Mikhaylik, Y. V.; Akridge, J. R. *J. Electrochem. Soc.* **2004**, *151*, A1969−A1976.
(7) Cheon, S. E.; Ko, K. S.; Cho, J. H.; Kim, S. W.; Chin, E. Y.; Kim, H. T. *J. Electrochem. Soc.* **2003**, *150*, A796−A799.
(8) Wang, J. L.; Yang, J.; Xie, J. Y.; Xu, N. X.; Li, Y. *Electrochem. Commun.* **2002**, *4*, 499−502.
(9) Ji, X.; Lee, K. T.; Nazar, L. F. *Nat. Mater.* **2009**, *8*, 500−506.
(10) Zheng, G.; Yang, Y.; Cha, J. J.; Hong, S. S.; Cui, Y. *Nano Lett.* **2011**, *11*, 4462−4467.
(11) Fu, Y.; Manthiram, A. *J. Phys. Chem. C* **2012**, *116*, 8910−8915.
(12) Simmonds, A. G.; Griebel, J. J.; Park, J.; Kim, K. R.; Chung, W. J.; Oleshko, V. P.; Kim, J.; Kim, E. T.; Glass, R. S.; Soles, C. L.; Sung, Y.; Char, K.; Pyun, J. *ACS Macro Lett.* **2014**, *3*, 229−232.
(13) Balsara, N. P.; Newman, J. *J. Chem. Educ.* **2013**, *90*, 446−452.
(14) Aurbach, D.; Zinigrad, E.; Cohen, Y.; Teller, H. *Solid State Ionics* **2002**, *148*, 405−416.
(15) Goodenough, J. B.; Kim, Y. *Chem. Mater.* **2010**, *22*, 587−603.
(16) Harry, K. J.; Hallinan, D. T.; Parkinson, D. Y.; MacDowell, A. A.; Balsara, N. P. *Nat. Mater.* **2014**, *13*, 69−73.
(17) Singh, M.; Odusanya, O.; Wilmes, G. M.; Eitouni, H. B.; Gomez, E. D.; Patel, A. J.; Chen, V. L.; Park, M. J.; Fragouli, P.; Iatrou, H.; Hadjichristidis, N.; Cookson, D.; Balsara, N. P. *Macromolecules* **2007**, *40*, 4578−4585.
(18) Panday, A.; Mullin, S.; Gomez, E. D.; Wanakule, N.; Chen, V. L.; Hexemer, A.; Pople, J.; Balsara, N. P. *Macromolecules* **2009**, *42*, 4632−4637.
(19) Mullin, S. A.; Stone, G. M.; Panday, A.; Balsara, N. P. *J. Electrochem. Soc.* **2011**, *158*, A619.
(20) Yuan, R.; Teran, A. A.; Gurevitch, I.; Mullin, S. A.; Wanakule, N. S.; Balsara, N. P. *Macromolecules* **2013**, *46*, 914−921.
(21) Teran, A. A.; Tang, M. H.; Mullin, S. A.; Balsara, N. P. *Solid State Ionics* **2011**, *203*, 18−21.
(22) Chintapalli, M.; Chen, X. C.; Thelen, J. L.; Teran, A. A.; Wang, X.; Garetz, B. A.; Balsara, N. P. *Macromolecules* **2014**, *47*, 5424−5431.
(23) Stone, G. M.; Mullin, S. A.; Teran, A. A.; Hallinan, D. T.; Minor, A. M.; Hexemer, A.; Balsara, N. P. *J. Electrochem. Soc.* **2012**, *159*, A222−A22717.
(24) Monroe, C.; Newman, J. *J. Electrochem. Soc.* **2005**, *152*, A396−A404.
(25) Newman, J.; Thomas-Alyea, K. E. *Electrochemical Systems*; John Wiley & Sons: New York, 2012.
(26) Pickering, T. T. *Sulfur in Organic and Inorganic Chemistry*; Marcel Dekker: New York, 1972.
(27) Barchasz, C.; Molton, F.; Duboc, C.; Leprêtre, J.-C.; Patoux, S.; Alloin, F. *Anal. Chem.* **2012**, *84*, 3973−3980.
(28) Kamyshny, A.; Goifman, A.; Gun, J.; Rizkov, D.; Lev, O. *Environ. Sci. Technol.* **2004**, *38*, 6633−6644.
(29) Wujcik, K. H.; Velasco-Velez, J.; Wu, C. H.; Pascal, T.; Teran, A. A.; Marcus, M. A.; Cabana, J.; Guo, J.; Prendergast, D.; Salmeron, M.; Balsara, N. P. *J. Electrochem. Soc.* **2014**, *161*, A1100−A1106.
(30) Chang, D. R.; Lee, S. H.; Kim, S. W.; Kim, H. T. *J. Power Sources* **2002**, *112*, 452−460.
(31) Agostini, M.; Hassoun, J. *Sci. Rep.* **2015**, 5.
(32) Teran, A.; Balsara, N. P. *Macromolecules* **2011**, *44*, 9267−9275.
(33) Chen, S.; Dai, F.; Gordin, M. L.; Wang, D. *RSC Adv.* **2013**, *3*, 3540−3543.
(34) Barghamadi, M.; Kapoor, A.; Wen, C. *J. Electrochem. Soc.* **2013**, *160*, A1256−A1263.
(35) Su, Y. S.; Fu, Y.; Cochell, T.; Manthiram, A. *Nat. Commun.* **2013**, DOI: 10.1038/ncomms3985.
(36) Pascal, T. A.; Wujcik, K. H.; Velasco-Velez, J. J.; Wu, C.-H.; Teran, A. A.; Kapilashrami, M.; Cabana, J.; Guo, J.; Salmeron, M.; Balsara, N. P. *J. Phys. Chem. Lett.* **2014**, *5*, 1547−1551.

DOI: 10.1021/acs.macromol.5b00928
Macromolecules 2015, 48, 4863−4873

(37) Hexemer, A.; Bras, W.; Glossinger, J.; Schaible, E.; Gann, E.; Kirian, R.; MacDowell, A.; Church, M.; Rude, B.; Padmore, H. *J. Phys. Conf. Ser.* **2010**, *247*, 012007.
(38) Ilavsky, J. *J. Appl. Crystallogr.* **2012**, *45*, 324−328.
(39) Huggins, R. *Ionics* **2002**, *8*, 300−13.
(40) Devaux, D.; Bouchet, R.; Gle, D.; Denoyel, R. *Solid State Ionics* **2012**, *227*, 119−127.
(41) Pielichowski, K.; Flejtuch, K. *Polym. Adv. Technol.* **2002**, *13*, 690−696.
(42) Li, X.; Hsu, S. L. *J. Polym. Sci., Part B: Polym. Phys.* **1984**, *22*, 1331−1342.
(43) Przylusky, J.; Wieczorek, W. *J. Therm. Anal.* **1992**, *38*, 2229−2238.
(44) Wieczorek, W.; Stevens, J. R.; Florjanczyk, Z. *Solid State Ionics* **1996**, *85*, 67−72.
(45) Lin, J. H.; Woo, E. M.; Huang, Y. P. *J. Polym. Sci., Part B: Polym. Phys.* **2006**, *44*, 3357−3368.
(46) Simon, F. T.; Rutherford, J. M. *J. Appl. Phys.* **1964**, *35*, 82−86.
(47) Minelli, M.; Baschetti, M. G.; Hallinan, D. T.; Balsara, N. P. *J. Membr. Sci.* **2013**, *432*, 83−89.
(48) MacCallum, J. R.; Vincent, C. A. *Polymer Electrolyte Reviews*; Elsevier Science: New York, 1987.
(49) Lascaud, S.; Perrier, M.; Vallke, A.; Besner, S.; Prud, J.; Armand, M. *Macromolecules* **1994**, *27*, 7469−7477.

DOI: 10.1021/acs.macromol.5b00928
Macromolecules 2015, 48, 4863−4873